Inorganic Chemistry

Article

Structure and Hydrolysis of the U(IV), U(V), and U(VI) Aqua Ions from Ab Initio Molecular Simulations

Raymond Atta-Fynn,*[,†] Donald F. Johnson,[†] Eric J. Bylaska,*[,†] Eugene S. Ilton,[‡] Gregory K. Schenter,[‡] and Wibe A. de Jong*[,†]

[†]Environmental Molecular Sciences Laboratory, and [‡]Chemical and Material Sciences Division, Pacific Northwest National Laboratory, P.O. Box 999, Richland, Washington 99352, United States

Supporting Information

ABSTRACT: Ab initio molecular dynamics simulations at 300 K, based on density functional theory, are performed to study the hydration shell geometries, solvent dipole, and first hydrolysis reaction of the uranium(IV) (U^{4+}) and uranyl(V) (UO_2^{+}) ions in aqueous solution. The solvent dipole and first hydrolysis reaction of aqueous uranyl(VI) (UO_2^{2+}) are also probed. The first shell of U^{4+} is coordinated by 8−9 water ligands, with an average U−O distance of 2.42 Å. The average first shell coordination number and distance are in agreement with experimental estimates of 8−11 and 2.40−2.44 Å, respectively. The simulated EXAFS of U^{4+} matches well with recent experimental data. The first shell of UO_2^{+} is coordinated by five water ligands in the equatorial plane, with the average U═O_{ax} and U−O distances being 1.85 Å and 2.54 Å, respectively. Overall, the hydration shell structure of UO_2^{+} closely matches that of UO_2^{2+}, except for small expansions in the average U═O_{ax} and U−O distances. Each ion strongly polarizes their respective first-shell water ligands. The computed acidity constants (pK_a) of U^{4+} and UO_2^{2+} are 0.93 and 4.95, in good agreement with the experimental values of 0.54 and 5.24, respectively. The predicted pK_a value of UO_2^{+} is 8.5.

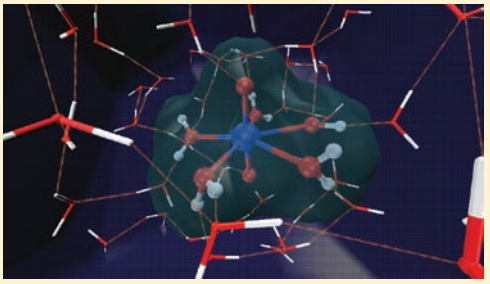

1. INTRODUCTION

Although U(VI) (UO_2^{2+}) is the most common uranium species in the environment, aqueous U(V) (UO_2^{+}(aq)) and U(IV) (U^{4+}(aq)) species may be important constituents of toxic uranium waste under strongly reducing conditions that are often present in deep geological repositories. Studies on the remediation of uranium-containing actinide waste have been largely focused on exploiting the vast differences in solubility between the soluble, mobile, U(VI) oxidation state and the less-soluble, less-mobile, reduced U(IV) oxidation state (UO_2(s)).[1] The reduction of U(VI) to U(IV) species has been shown to be driven by microbial organisms,[2−10] mineral surfaces,[11−15] and photochemical processes.[16−19] The first step in the reduction of aqueous UO_2^{2+} is generally thought to be a fast one-electron reduction reaction,

$$e^- + UO_2^{2+}(aq) \rightleftharpoons UO_2^{+}(aq)$$

resulting in a UO_2^{+}(aq) intermediate. This is then followed by disproportionation to U(IV) and U(VI) species. However, U(V) can be stabilized by various organic ligands or in concentrated aqueous carbonate solutions and nonaqueous solutions.[20−30] Unfortunately, experiments have not searched for, nor identified, U(V) under environmentally relevant conditions, since the disproportionation reaction is assumed to render U(V) insignificant. It is also possible that, under strongly reducing conditions, U(V) might never be produced, because aqueous U(IV) species could be formed by a direct $2e^-$ transfer to U(VI). Nevertheless, the recent discovery that U(V) can be a high proportion of U incorporated in solid phases under a broad range of environmentally relevant conditions[11,31] suggests that UO_2^{2}(aq) may form a non-negligible percentage of aqueous U over a wider range of Eh and pH than previously considered. Consequently, a more thorough understanding of UO_2^{+}(aq) and U^{4+}(aq) is not only of fundamental interest but is potentially relevant to determining the fate and transport of U in the environment.

The solvent shell properties of UO_2^{2+} in various aqueous environments have been extensively studied both theoretically and experimentally (see Nichols et al.[32] and the references therein for past theoretical and experimental studies on UO_2^{2+}(aq)). The solvent shell structure of UO_2^{+} is thought to be similar to UO_2^{2+}, but there are no published experimental data. Experimental data also indicates that UO_2^{2+} is a fairly weak acid in aqueous solution (pK_a values are 5.24 ± 0.25,[33] 5.58 ± 0.24[34]), whereas the acidity of UO_2^{+} in aqueous solution is unknown. Only a few experimental studies have been published on structurally similar XO_2^{+} ions (X denotes an actinide metal): an extended X-ray absorption fine spectra (EXAFS) study of aqueous NpO_2^{+}[35] and X-ray absorption near edge structure (XANES) studies of aqueous PuO_2^{+}.[36,37] These studies suggest that the first shell of NpO_2^{+} contains five water ligands in the equatorial plane (similar to the first shell

Received: October 28, 2011
Published: February 16, 2012

   dx.doi.org/10.1021/ic202338z | *Inorg. Chem.* 2012, 51, 3016−3024

structure of UO_2^{2+}), while the first shell of PuO_2^{+} contains four ligands in the equatorial plane.

There is a fair amount of theoretical gas-phase predictions on the geometries of UO_2^{+} and $[UO_2(OH_2)_5]^{+}$.[38−44] Calculations on bare UO_2^{+} predicted the axial bond distance, U═O_{ax}, to be 1.77−1.78 Å at the CASSCF/CASPT2 level of theory,[38] and 1.76−1.81 Å using relativistic density functional theory (DFT).[38,42,43] The predicted U═O_{ax} and U−O_{eq} (equatorial) distances in $[UO_2(OH_2)_5]^{+}$ are 1.81−1.89 Å and 2.44−2.62 Å, respectively, at the relativistic density functional theory (DFT) level of theory,[39,40,42] and 1.81 Å and 2.51 Å, respectively, at the unrestricted second-order Møller−Plesset (UMP2) level of theory.[41] Using $[UO_2(OH_2)_5]^{+}(OH_2)$ in a polarizable continuum model (PCM) solvent and Hartree−Fock (HF) level of theory, the water exchange mechanism was predicted to be dissociative with an activation energy of 36 kJ/mol, and the U═O_{ax} and U−O_{eq} distances were 1.78 Å and 2.62 Å, respectively.[44] A HF quantum mechanical/molecular mechanics (QM/MM) simulation of fully solvated UO_2^{+} predicted a first-shell coordination number of 4, and U═O_{ax} and U−O_{eq} distances of 1.78 Å and 2.51 Å, respectively.[45]

Possible first-shell coordination numbers of aqueous U^{4+} measured in experiments range from 8 to 11.[46−49] Large-angle X-ray scattering (LAXS) studies on the coordination shell structure of U^{4+} in aqueous solution indicated that the first coordination number is 8.2 ± 0.4.[46,47] EXAFS studies of U^{4+} in 1.5 M $HClO_4$ acid yielded a first-shell coordination number of 10 ± 1.[48] A more recent EXAFS study of U^{4+} in 1 M $HClO_4$ acid yielded a first-shell coordination number of 9−10.[49] Relativistic DFT calculations on $[U(OH_2)_n]^{4+}$ (n = 8, 9, 10) gas-phase clusters yielded the most stable hydrate to be $[U(OH_2)_9]^{4+}$ with a trigonal tricapped prism (TTP) water geometry and an average U−O bond distance of 2.49 Å.[50] Calculations of the U L_{III}-edge XANES of $[U(OH_2)_n]^{4+}$ (n = 8, 9, 10) clusters showed that the spectra of $[U(OH_2)_9]^{4+}$, with the water molecules arranged in a TTP geometry, yielded the best match with the experiment.[51] HF−QM/MM simulation of U^{4+}(aq) predicted a first-shell coordination of 9 and average U−O distance of 2.45 Å.[52] Experimental studies have shown that U^{4+} is a strong acid in solution with a first acidity constant of 0.54 ± 0.06.[33]

The most reliable route to accurate predictive modeling of strongly interacting systems such as charged actinide ions and molecules in solution is a direct simulation at the molecular level with no adjustable parameters (i.e., ab initio modeling). In this paper, ab initio molecular dynamics (AIMD) simulations have been used to (i) determine the hydration shell geometries of U^{4+} and UO_2^{+} and (ii) compute the solvent dipole moments and first acidity constants of U^{4+}, UO_2^{+}, and UO_2^{2+}. AIMD simulations of the hydration-shell geometry of UO_2^{2+}(aq) has been carried out in a previous study[32] and will be used here for the purposes of comparison to UO_2^{+}(aq). The remainder of the article is organized as follows. First, the computational methodology used in this work is described. Then, the results of the simulations and a discussion of the coordination shell geometry, EXAFS, dipole moments of the solvating water molecules, and the first hydrolysis mechanisms are presented; the results are compared to available theoretical and experimental data. Finally, a summary and conclusions of the work are presented.

2. COMPUTATIONAL METHODS

2.1. AIMD Simulations. Car−Parrinello molecular dynamics (CPMD)[53] simulations in the canonical ensemble at 300 K were performed for UO_2^{+} and U^{4+}, using the pseudo-potential plane-wave density functional theory (DFT)[54] module implemented in the NWChem code.[55] Each simulation employed 1 ion and 64 water molecules in a periodic cubic cell 12.4 Å in length (water density ≈ 1 g/cm^3). The charges on the metal centers were compensated with uniform background charges of opposite sign and equal magnitude. The Perdew−Burke−Ernzerhof (PBE) generalized gradient approximation[56] to the exchange-correlation functional was employed. Electron-ion interactions were treated with norm-conserving pseudopotentials modified into a separable form due to Kleinman and Bylander.[57] Hamann-type pseudo-potentials[58,59] were employed for hydrogen and oxygen, and Troullier−Martins[60] pseudo-potentials were employed for uranium. The details of the pseudo-potentials have been described elsewhere.[32] The Kohn−Sham wave functions and charge density were expanded using plane waves basis up to a kinetic energy cutoffs of 120 and 240 Ry, respectively. The $\Gamma(\vec{k} = 0$ point was used to sample the Brillouin zone in all simulations. The temperature was controlled using the Nose−Hoover thermostat.[61,62] To facilitate the numerical integration, the H atoms were replaced with deuterium (D). A fictitious electronic mass of 600 au and a simulation time step of δt = 5 au (0.121 fs) were employed. Each system was initially equilibrated for 8 ps using a QM/MM potential,[63] followed by a further CPMD equilibration for 3 ps. Configurations from the post-equilibration CPMD simulations were saved at time intervals of 10δt. The total collection times were 17 000δt (20.6 ps) for UO_2^{+}(aq) and 18 000δt (21.8 ps) for U^{4+}(aq).

2.2. Metadynamics Simulations. To compute the first hydrolysis constant, the free energy (ΔF) of hydrolysis is required. Common approaches to computing ΔF are the free-energy perturbation method,[64] thermodynamic integration,[65,66] umbrella sampling,[67] and metadynamics.[68−70] We employed ab initio metadynamics to compute ΔF at 300 K for UO_2^{+}(aq), UO_2^{2+}(aq), and U^{4+}(aq). If the simulated hydrolysis constant of UO_2^{2+}(aq) matches well with the experiment, then we will deem the predicted result for UO_2^{+}(aq) to be reliable.

Metadynamics[68−70] is a nonequilibrium molecular dynamics method that accelerates the sampling of the multidimensional free-energy surfaces of chemical reactions on a short-to-moderate simulation time scale. The accelerated sampling is achieved by adding an external history (that is, time-dependent) bias potential, which is a function of the collective variables (Ξ) to the Hamiltonian of the system. Ξ is a generic function of the system coordinates (e.g., bond distance, bond angle, etc.) that can distinguish between reactants and products and can sample the low-energy reaction paths. The history potential is adaptively added to the Hamiltonian by "flooding" the energy landscape with repulsive Gaussian "hills" centered on the current location of Ξ at a constant time interval of τ_G. Suppose that prior to any time t during a metadynamics simulation, M repulsive Gaussians centered on $\Xi_{t'}$ are deposited along the trajectory of Ξ at times $t' = \tau_G, 2\tau_G, ..., M\tau_G$. The history potential $V(\xi,t)$, at an arbitrary value ξ, of Ξ at time t then is given by

$$V(\xi, t) = \sum_{\substack{t'=\tau_G,2\tau_G,\ldots \\ t'<t}} H_G \exp\left(\frac{|\xi - \Xi_{t'}|^2}{2\omega^2}\right) \quad (1)$$

where H_G and ω are, respectively, the height and width of the Gaussian hill. The accumulation of the history potential low-energy regions allows the system to cross energy barriers much more quickly, effectively encouraging the system to explore new regions of Ξ.

The basic assumption of metadynamics is that, after a sufficiently long time, $V(\xi,t)$ cancels the underlying free energy surface $F(\xi)$ along Ξ:

$$F(\xi) \approx -\lim_{t\to+\infty} V(\xi, t) + \text{constant} \quad (2)$$

dx.doi.org/10.1021/ic202338z | Inorg. Chem. 2012, 51, 3016−3024

Using the metadynamics estimates for ΔF, the acid dissociation constant (pK_a) is computed using the standard definition

$$pK_a = \frac{\Delta F}{RT \ln 10} \quad (3)$$

Here, the collective variable that we employ to describe the deprotonation of a first-shell water is the coordination number, $\xi(|\mathbf{r}_{O_IH}|)$, of a specific first-shell water oxygen atom (O_I), with respect to all protons:[71]

$$\xi(|\mathbf{r}_{O_IH}|) = \sum_{i=1}^{N_H} \frac{1}{1 + \exp[\kappa(|\mathbf{r}_{O_IH_i}| - r_{cut})]} \quad (4)$$

where N_H is the total number of protons, r_{cut} the O−H cutoff distance, and κ an arbitrary positive constant chosen to reproduce the equilibrium coordination number (see the Supporting Information for the rationale for our choice of this collective variable).

Starting with equilibrated CPMD geometries of UO_2^+(aq), UO_2^{2+}(aq), and U^{4+}(aq), the metadynamics simulations were carried out at 300 K with H_G = 0.0001 au (0.063 kcal/mol), $\omega = 0.1/(2^{1/2})$, κ = 10 Å^{-1}, and r_{cut} = 1.38 Å. For U^{4+}(aq), $\tau_G = 100\delta t$; for UO_2^{2+}(aq) and UO_2^+(aq), $\tau_G = 20\delta t$ [τ_G is smaller for UO_2^{2+}(aq) and UO_2^+(aq), since their deprotonation energies are expected to be greater than that of U^{4+}(aq)].

3. RESULTS AND DISCUSSION

3.1. Hydration Shell Structure. *UO_2^+(aq).* In the top panel of Figure 1, the radial distribution function (RDF) and running coordination numbers of UO_2^+ are shown. Well-defined and isolated peaks in the RDF can be seen in the 1.5−2.0 Å range for the U═O_{ax} molecular bonds, and in the 2.2−3.0 Å range for the first hydration shell. Table 1 lists the structural properties of the hydration shell of UO_2^+. For the purposes of comparison, past experimental and theoretical data for the first shell of AnO_2^+ (An = U, Np, Pu) and UO_2^{2+} (ref 32) are also reported in Table 1. Our first-principles simulations indicate that the first shell of UO_2^+ has five water molecules in the equatorial plane (cf. Figure 2), in contrast to the QM/MM prediction of 4.[45] Our predicted U═O_{ax} distance is very close to previous measurements of other actinyl(V) ions (NpO_2^+ and PuO_2^+) and are greater than the previous predicted value[45] by 0.07 Å (cf. Table 1). Also, our average first-shell U−O_{eq} bond distance is slightly longer than the previous simulated value,[45] which is expected since the first shell of our simulation contains more water ligands. Previous gas-phase structures exhibit slightly longer U−O_{eq} bonds as expected.[39,40,42,44] Relative to UO_2^{2+}(aq),[32] UO_2^+(aq) shows a lengthening of 0.08 Å and 0.1 Å for the U═O_{ax} and U−O_{eq} bonds, respectively, because of reduced electrostatic attraction. Other first-shell properties of UO_2^+ and UO_2^{2+}, such as the intramolecular water geometry and tilt angles, compare closely.

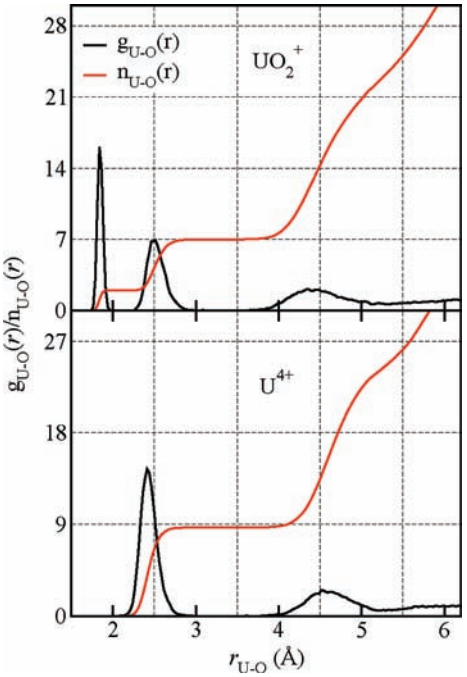

Figure 1. Partial U−O radial distribution function (RDF) $gU{-}O(r)$ and running coordination number $n_{U-O}(r)$ for UO_2^+ (aq) (upper panel) and U^{4+}(aq) (lower panel).

Figure 1 shows a well-defined second shell in the 3.5−5.2 Å range for UO_2^+(aq) with an average U−O_{II} distance of 4.55 Å. HF-QM/MM simulation of UO_2^+(aq) did not yield a well-defined second-shell structure, and the average U−O_{II} distance was not reported.[45] The data in Table 2 indicates that the second shell of UO_2^+ contains an average of 15.4 ligands, which is much larger than the QM/MM value of 12.4.[45] The second solvation shell is further characterized by quantifying the water populations in the equatorial and apical regions (cf. Table 2). The equatorial region consists of second-shell water molecules that form acceptor hydrogen bonds with first-shell water donors, while the remaining second-shell waters form the apical region. There are 8−9 water molecules in the equatorial region, which compares closely to the value of 9−10 from the AIMD simulation of UO_2^{2+}(aq).[32] There are 6−7 waters molecules in the apical region, 4 of which form donor hydrogen bonds with the 2 O_{ax} acceptor atoms (2 hydrogen bonds per O_{ax}). In fact, the average values of $\angle_{O_IH_IO_{II}}$ angle and $R_{O_I-O_{II}}$ reported in Table 2 are indicative of a well-defined hydrogen bonding network between the first and second hydration shells.

A visual description of the hydrogen bonding between the first and second solvent shells of UO_2^+ is presented in Figure 2. The hydrogen bonds between the five first-shell waters and nine equatorial second-shell waters can clearly be seen. Also depicted are the hydrogen bonds formed between four apical second-shell waters and the two axial oxygens (solid black bonds). The remaining apical second-shell waters form hydrogen bonds with either the equatorial second-shell or bulk waters. These features are consistent with the results of AIMD simulations of the hydration shell structure of UO_2^{2+}.[32] However, our result, that there are two hydrogen bonds per axial oxygen, contradicts QM/MM simulations that found only one hydrogen bond per axial oxygen.[45] The computed mean residence times of water in the equatorial and apical second shells were 17.4 and 8.9 ps, respectively (based on a minimum survival time of t^* = 0.5 ps), implying that the equatorial region is more stable than the apical region. The large average tilt angle of ∼35° (see Table 1) indicates a tetrahedral character in the hydrogen bonding network near the first shell (see the Supporting Information for detailed analysis of the hydrogen bonding network).

U^{4+}(aq). In the lower panel of Figure 1, the RDF and running coordination number of U^{4+}(aq) are depicted. The first and second hydration shell parameters are reported in Table 3. The first-shell coordination number is 9 for the first 15.2 ps (this corresponds to a frequency of 70%) and 8 for the remaining 6.4 ps (with a frequency of 30%), resulting in an average first-shell coordination number of 8.7, which lies on the

dx.doi.org/10.1021/ic202338z | Inorg. Chem. 2012, 51, 3016−3024

Table 1. Average First Hydration Shell Parameters of AnO_2^+ (An = U, Np, Pu) and UO_2^{2+} in Aqueous Solution and Gas Phase

	ref(s)	N_{H_2O}[a]	$R_{An=O_{ax}}$ (Å)[b]	$\angle_{O_{ax}AnO_{ax}}$ (deg)[c]	$R_{An-O_{eq}}$ (Å)[d]	$R_{O_{eq}-H}$ (Å)[e]	$\angle_{HO_{eq}H}$ (deg)[f]	$\angle_{tilt}$ (deg)[g]
UO_2^+ (aq)[h]	this work	5	1.85	174	2.54	0.97	106.6	34.9
UO_2^+ (aq) (QM/MM)	45	4	1.78	177	2.51			
$[UO_2(H_2O)_5]^+$	39	5	1.81		2.62			
$[UO_2(H_2O)_5]^+$	40	5	1.82−1.83		2.57−2.62			
$[UO_2(H_2O)_5]^+$	42	5	1.82		2.56−2.58			
$[UO_2(H_2O)_5]^+$ (H_2O)	44	5	1.78		2.62			
NpO_2^+ (aq) (EXAFS)	35	5	1.85		2.51			
PuO_2^+ (aq) (XANES)	36, 37	4	1.84		2.45			
UO_2^{2+} (aq)	32	5	1.77	174	2.44	0.98	107.6	32.9

[a]Number of water molecules in the first coordination shell. [b]An=O_{ax} bond distance, where O_{ax} denotes an axial O atom bonded to An. [c]O_{ax}=An=O_{ax} bond angle. [d]An−Oeq bond distance, where "eq" denotes a first shell water in the equatorial plane of UO_2^+. [e]O_{eq}−H bond distance. [f]H−O_{eq}−H bond angle. [g]Tilt angle of first-shell water molecules, with respect to the An−O bonds, computed as $\angle_{tilt} = \cos^{-1}\{(R_{U-H}^2 - R_{U-O_{eq}}^2 - R_{O_{eq}-H}^2)/[2R_{U-O_{eq}}R_{O_{eq}-H}\cos(\theta/2)]\}$, where $\theta = \angle_{HO_{eq}H}$. [h]First-shell parameters were based on a cutoff of $R_{An-O_{eq}} < 3.5$ Å.

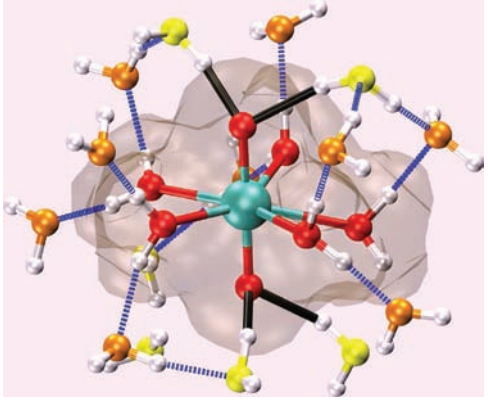

Figure 2. Snapshot of the first shell (partially clothed region) and second shell of UO_2^+ (aq). Legend: The first shell oxygens are colored red, the equatorial second shell oxygens are colored orange, and the apical second shell oxygens are colored yellow; the black bonds denote the hydrogen bonds between axial oxygens O_{ax} and the apical second shell waters.

low end of the experimental range of 8−11.[46−49] Our reported value is less than the value of 9 from a 9-ps QM/MM simulation.[52] Based on the experimental mean residence time of a first-shell water molecule of U^{4+}(aq), which was determined to be 170−210 ns,[72] it is highly likely the first-shell coordination number in our simulation will stay at 8 if the simulation is allowed to proceed for long times (several picoseconds to nanoseconds). Hence, the initial coordination number of 9 is probably a metastable state. The underestimation of the first-shell coordination number of actinide ions appears to be a generic problem with DFT-GGA. For example, experiments predict a coordination number of several trivalent actinide ions to be 9 while DFT-GGA predicts 8 (see, for example, Wiebke et al.[73] and Atta-Fynn et al.[74]). While the simulations employed no perchlorate counter-anions, it is possible that their inclusion could alter the equilibrium coordination number.[75] It should also be pointed out that the error margin in the EXAFS determination of the first-shell coordination number is ±10%−15%; hence, our coordination number lies well within the experimental limits. Furthermore, DFT-GGA methods are known to overestimate bond lengths in actinide compounds.[76] The average U−O bond distance is consistent with the QM/MM value[52] but slightly overestimated by 0.03−0.05 Å, compared to the experimental values.

The average geometric arrangement of the first-shell water molecules around U^{4+} can be deduced by comparing the simulated average O−U−O angular distribution function (ADF) to ideal (crystalline) 8-fold and 9-fold coordinated hydrates. Our comparisons indicated that the dominant simulated $[U(OH_2)_8]^{4+}$ geometry is square antiprismatic (SAP), while the dominant $[U(OH_2)_9]^{4+}$ geometry is tricapped trigonal prism (TTP). The results are shown in Figure 3. In the top panel, the average ADF of the simulated $[U(OH_2)_8]^{4+}$ and $[U(OH_2)_9]^{4+}$ geometries are compared to an ideal SAP; in the lower panel, comparisons have been made to an ideal TTP. The agreements can be seen in the match in the peak positions. The TTP geometry of $[U(OH_2)_9]^{4+}$ predicted here is in accordance with QM/MM results.[52] Note that, in both graphs, the peaks in the 90°−120° range are not clearly reproduced, because of severe geometrical distortions stemming from thermal effects. In Figures 4a and 4b, respective representative snapshots of distorted TTP and SAP geometries from the simulations are depicted. These geometries have been observed in lanthanide and other actinide ions[77] (see also Atta-Fynn et al.[74] for a description of the geometries).

The average second-shell coordination number of U^{4+}(aq) is 15.2 (see Table 3), which is less than the QM/MM value of 19.[52] As a result, the average QM/MM second shell U−O distance is 0.15 Å longer than our AIMD value. The average

Table 2. Average Second Hydration Shell Parameters of UO_2^+ and UO_2^{2+} in Aqueous Solution[a]

		Entire Shell				Equatorial Shell			Apical Shell		
	ref	N_{H_2O}	$R_{U-O_{II}}$[b] (Å)	$R_{O_I-O_{II}}$[c] (Å)	$\angle_{O_IH_IO_{II}}$ (deg)	N_{H_2O}	$R_{U-O_{II}}$ (Å)	$R_{O_I-O_{II}}$ (Å)	N_{H_2O}	$R_{U-O_{II}}$ (Å)	$R_{O_I-O_{II}}$ (Å)
UO_2^+ (aq)[d]	this work	15.4	4.55	2.84	161.8	8.5	4.57	2.81	6.9	4.53	3.06
UO_2^+(aq)	45	12.4									
UO_2^+(aq)	32	14.8	4.45	2.72	163.5	9.7	4.45	2.71	5.1	4.43	2.88

[a]Defintion of parameters is the same as in Table 1. [b]Subscript II denotes a second-shell oxygen. [c]Subscript I denotes a first-shell oxygen. [d]Second-shell parameters were based on a cutoff of 3.5 Å ≤ $R_{U-O_{II}}$ < 5.2 Å.

dx.doi.org/10.1021/ic202338z | Inorg. Chem. 2012, 51, 3016−3024

Table 3. Average First and Second Hydration Shell Parameters of U^{4+} in Aqueous Solution[a]

First-Shell Parameters[b]							
ref(s)	method	N_{H_2O}	R_{U-O_I} (Å)[c]	R_{U-H_I} (Å)	$R_{O_I-H_I}$ (Å)	$\angle_{H_IO_IH_I}$ (deg)	$\angle_{tilt}$ (deg)
this work		8.7[d]	2.45	3.09	0.98	106.4	24.6
52	QM/MM	9	2.45	3.1[d]			
47	LAXS	7.8–8.6	2.44				
48, 49	EXAFS	9–11 (ref 48), 9–10 (ref 49)	2.42 (ref 48), 2.40 (ref 49)				
Second-Shell Parameters[e]							
ref	method	N_{H_2O}	$R_{U-O_{II}}$ (Å)[f]	$R_{U-H_{II}}$ (Å)	$R_{O_I-O_{II}}$ (Å)	$\angle_{O_IH_IO_{II}}$ (deg)	
this work		15.2	4.65	5.04	2.81	161.8	
52	QM/MM	19	4.80				

[a]Definition of parameters is the same as that given in Table 1. [b]First-shell parameters were based on a cutoff of $R_{U-O_I} < 3.5$ Å. [c]Subscript I denotes a first-shell water molecule. [d]Estimated from the U–H RDF by Frick et al.[52] [e]Second-shell parameters were based on a cutoff of 3.5 Å $\leq R_{U-O_{II}} <$ 5.2 Å. [f]Subscript II denotes a second-shell water molecule.

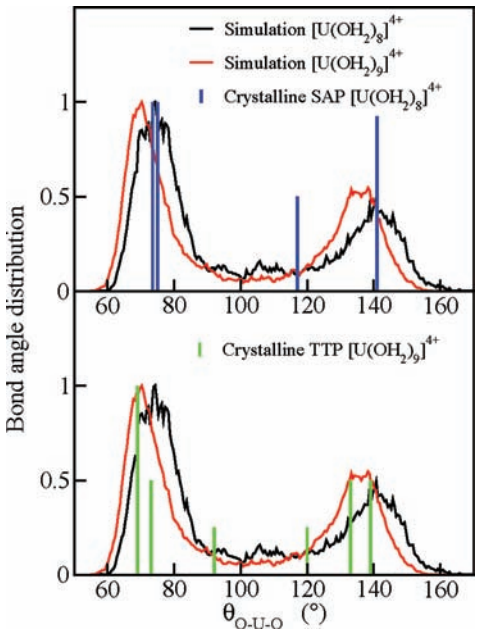

Figure 3. Comparison of the average $O-U^{4+}-O$ angular distribution function (ADF) for 8-fold ($[U(OH_2)_8]^{4+}$) and 9-fold coordinated ($[U(OH_2)_9]^{4+}$) first shells to ideal crystalline hydrates.

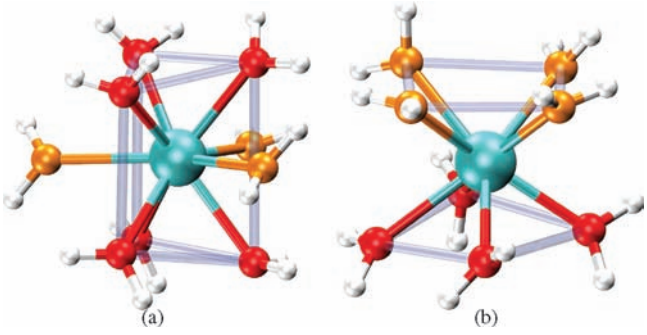

Figure 4. Representative first-shell geometry of U^{4+}(aq): (a) 9-fold trigonal tricapped prismatic (TTP) water geometry and (b) 8-fold square antiprismatic (SAP) water geometry.

values of 162° and 2.81 Å for the $\angle_{O_IH_IO_{II}}$ angle and $R_{O_I-O_{II}}$ distance, respectively, are signatures of a well-defined hydrogen bonding network between the first and second hydration shells. Hydrogen bonding analysis indicated that the first-shell waters of U^{4+}(aq) are trigonally bound to the second-shell waters; that is, the first-shell water act mainly as donors to the second-shell water (see the Supporting Information for additional discussions). The trigonal behavior stems from the relatively small tilt angles (~25° in Table 3) of the first-shell water molecules.

3.2. EXAFS. Often, in the theoretical modeling of ions in aqueous solution, the average geometric quantities (coordination numbers, bond distances, and angles) are used to determine the agreement between theory and experiment. In some cases, however, this is may not be sufficient to fully validate the reliability of the model. Here, we go a step further by comparing a key structural property—namely, the EXAFS—of our simulated models to available experimental data. The U L_{III}-edge EXAFS is computed using FEFF9 ab initio multiple scattering code,[78,79] and the molecular dynamics EXAFS (MD-EXAFS) method[80] (see the Supporting Information for a description of the method).

UO_2^+(aq). There is no experimental EXAFS data for UO_2^+; therefore, the simulated EXAFS is a prediction that could be useful to experimentalists. It has been shown elsewhere, using the MD-EXAFS method, that the spectra of UO_2^{2+} from AIMD[32] agrees well with recent experimental data.[35] In Figure 5, the $k^3\chi(k)$ of UO_2^+ (top panel), and the magnitude of Fourier transform of $k\chi(k)$ (bottom panel) are depicted (phase-shift corrections were not included in the radial distances). There is a stark similarity between the UO_2^+ EXAFS and the reported theoretical and experimental spectra for UO_2^{2+}(aq).[32,35] This is obviously due to the similarities in coordination shell geometries and RDFs.

U^{4+}(aq). In Figure 6, plots of the simulated $k^3\chi(k)$ EXAFS (top panel) and $|\overline{\chi}(R)|$ (bottom panel) are depicted and compared with recent experimental data for 0.05 M U^{4+} in a 1 M $HClO_4$ solution.[49] As can be seen in the top panel in Figure 6, the simulated spectrum almost matches the frequency and amplitude oscillations of the experimental curve. The agreement can also be seen in the Fourier-transformed data in the bottom panel in Figure 6. The central peak mismatch in the bottom panel in Figure 6 is due to the fact that the simulated average $U-O_I$ distance is longer than the corresponding experimental value. Older EXAFS data for 0.05 M U^{4+} in 1.5 M $HClO_4$[48] were compared to our spectrum and the recent experimental data;[49] some differences were observed, the source of which is not clearly known (see the Supporting Information for the comparisons).

dx.doi.org/10.1021/ic202338z | Inorg. Chem. 2012, 51, 3016–3024

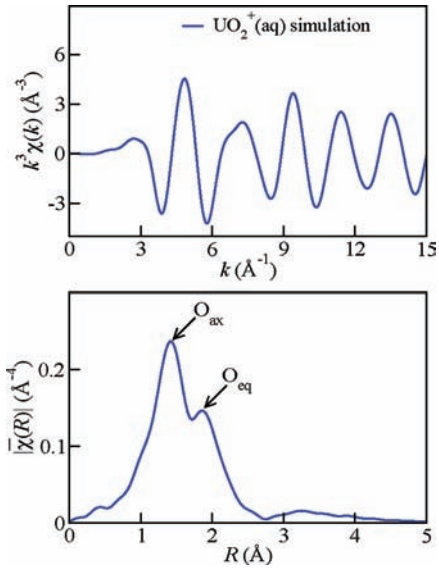

Figure 5. Simulated EXAFS spectra of UO_2^+ (aq). The upper panel shows a $k^3\chi(k)$ EXAFS spectrum; the lower panel shows the magnitude of the Fourier transform, $|\overline{\chi}(R)|$, of $k\chi(k)$.

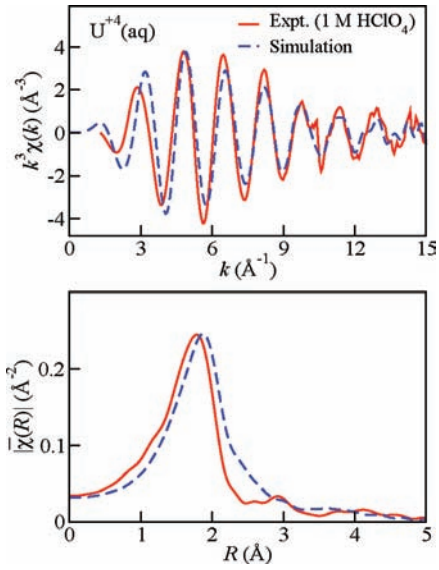

Figure 6. Comparison of the simulated and experimental EXAFS spectra of U^{4+}(aq).[49] The upper panel shows the $k^3\chi(k)$ EXAFS spectra; the lower panel shows the magnitude of the Fourier transform $|\overline{\chi}(R)|$.

3.3. Dipole Moments of the Solvating Water Molecules. Here, we compare the trends in the polarization of water by U^{4+}, UO_2^+, and UO_2^{2+}. In Table 4, the dipole moments per water ligands in the first-shell, second-shell, and bulk regions of each cation are reported. The dipole moments were computed using the maximally localized Wannier–Boys orbital technique[81−84] and averaged over 20 uniformly spaced (with respect to the simulation time) snapshots. The trajectory from a previous AIMD simulation[32] was used for the UO_2^{2+} dipole moment calculations. In Figure 7a, the average location of each doubly occupied Wannier function centers (WFC) in a water molecule is shown; the lone pair orbitals (LPO) are colored yellow and the bonding orbitals (BO) are colored green. In Figure 7b, the distributions of the radial distances between the O atoms from their respective WFCs are depicted for U^{4+} and UO_2^+.

Table 4. Dipole Moments of the Water Molecules in the First-Shell, Second-Shell, and Bulk Regions of U^{4+}(aq), UO_2^+(aq), and UO_2^{2+} (aq)

	Dipole Moment (D)		
	first shell	second shell	bulk region
U^{4+}(aq)	4.2 ± 0.5	3.0 ± 0.3	2.9 ± 0.3
UO_2^+(aq)	3.5 ± 0.3	2.9 ± 0.3	2.9 ± 0.3
UO_2^{2+}(aq)	4.1 ± 0.4	2.9 ± 0.3	2.8 ± 0.3

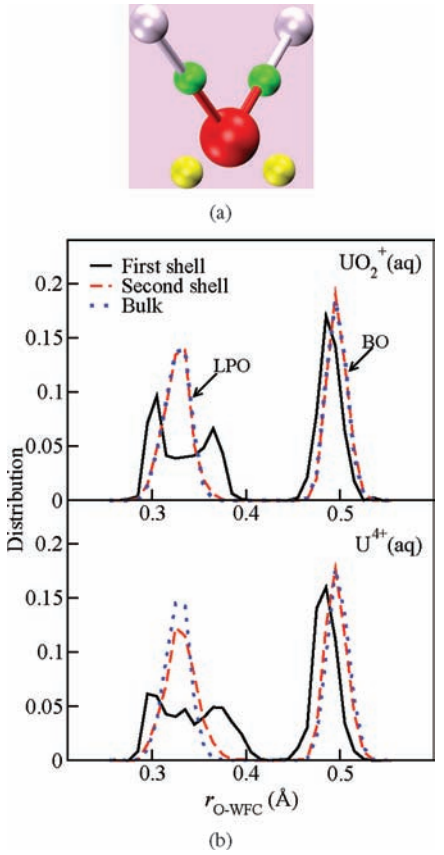

Figure 7. (a) Depiction of the location of the lone-pair orbitals (LPO) and bonding orbitals (BO) Wannier function centers (WFC) in the water molecule. LPO is colored yellow and BO is colored green. (b) Distributions of the distances, r_{O-WFC}, between the oxygen atoms and the WFC per water molecule for first, second, and bulk solvent shells.

UO_2^+ and UO_2^{2+}. The electric field of UO_2^+ is quite strong, and it polarizes the first-shell water by an average +0.6 D, relative to the average bulk water dipole moment of 2.9 D (cf. Table 4). The average second-shell water dipole moment is no different from the bulk implying that polarization effects do not extend beyond the first shell. According to Figure 7b, the distribution of LPO−O distance is bimodal (centered on 0.3 and 0.36 Å), while the second-shell and bulk distributions each have a single well-defined center, similar to liquid water.[85] The bimodal distribution is due to the asymmetric (tilt) orientation of a water molecule around the ion, resulting in one LPO being pulled away from the O atom toward the ion and the other being pulled closer.[86] The asymmetric orientation is a

dx.doi.org/10.1021/ic202338z | Inorg. Chem. 2012, 51, 3016−3024

consequence of the large first-shell dipole tilt angle of 35° due to the hydrogen-bond formation with the water molecules in the second and bulk solvation shells and the UO_2^+–H_2O electrostatic interaction. UO_2^{2+} polarizes the first water ligands much more strongly than UO_2^+. The shift in the UO_2^{2+} first-shell dipole moments is at least 1.2 D, relative to the second-shell and bulk water dipole moments. Furthermore, the trends in the distributions of LPO–O distances in UO_2^{2+}(aq) are similar to that of UO_2^+.

U^{4+}. The data in Table 4 show a large dipole moment shift of 1.2 D in average dipole moment of the first-shell water molecules around U^{4+}, relative to the bulk. The shift is similar to that of UO_2^{2+}, even though they differ by two charge units (intuitively, one would expect the +4 center to polarize the solvent more strongly than the +2 center). However, U^{4+} (UO_2^{2+}) polarizes 8–9 (5) water molecules; therefore, it has a stronger polarizing effect on the first shell. The second shell exhibits a small polarization of 0.1 D, relative to the bulk. The asymmetric distribution of the O–LPO distances observed for UO_2^+ is also evident in U^{4+} (Figure 7b, lower panel). However, the peak splitting features are not as well-defined, compared to the case of UO_2^+. This is due to the comparatively large tilt angles of the UO_2^+ first-shell water molecules.

3.4. First Acidity Constant from the Metadynamics Simulations. For a metal ion in aqueous solution, hydrolysis occurs when partial charge transfer from a first-shell water molecule to the metal makes the molecule a sufficient Brønsted–Lowry acid to promote a proton transfer to the second shell.[77] The first hydrolysis reactions of U^{4+} and UO_2^+ are given by

$$[U(OH_2)_8]^{4+} + H_2O \rightleftharpoons [U(OH_2)_7(OH)]^{3+} + H_3O^+$$

$$[UO_2(OH_2)_5]^+ + H_2O \rightleftharpoons UO_2(OH_2)_4(OH) + H_3O^+$$

The deprotonated species can form a mixture of new aqua species and precipitates, depending on the pH and other thermodynamic conditions. Therefore, knowledge of the hydrolysis of actinide ions in aqueous solution enhances our ability to accurately predict the chemistry and thermodynamics of nuclear waste remediation. For highly charged actinide ions in solution, e.g., U^{4+}, hydrolysis occurs with ease, since the strong ion–oxygen electrostatic attraction and charge transfer from the first-shell water $3a_1$ orbital (σ orbital containing the O lone pair electrons) to empty *d* orbitals of U weakens the O–H bond, leading to the release of H^+. Because of its high charge, U^{4+} is expected to be a much stronger acid in aqueous solution than UO_2^+ and UO_2^{2+}. In fact, the measured acid dissociation constant, pK_a, of U^{4+}(aq) is pK_a = 0.54 ± 0.06, while that of UO_2^{2+} are 5.24 ± 0.25 (ref 33) and 5.58 ± 0.24 (ref 34).

Analyses of the proton-transfer mechanisms in U^{4+}(aq), UO_2^+(aq) and UO_2^{2+}(aq) from the metadynamics simulations are presented in the Supporting Information. In all cases, there was no cooperativity during or after the proton transfer; that is, no water molecule departed from the first shell during hydrolysis. Here, we focus on the deprotonation free energy differences of each system.

U^{4+}(aq). In Figure 8, the reconstructed free-energy profile (black curve) is shown, where the reactant free energy is taken as the zero reference point. The figure shows that the free-energy difference between the reactant ($\xi \approx 2$) and the product ($\xi \approx 1$) is $F(\xi = 1) - F(\xi = 1.97)$ = 2.52 kcal/mol. Since any of the 8 independent first-shell water molecules could have been

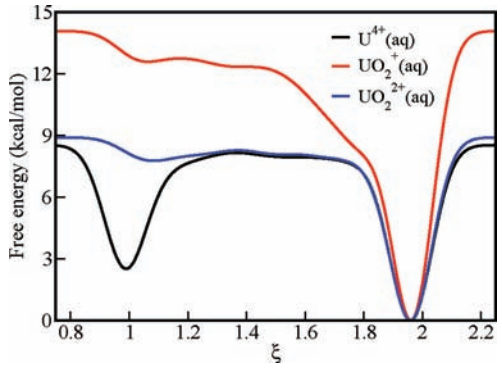

Figure 8. Free-energy profiles of the deprotonation of U^{4+}(aq), UO_2^+(aq), and UO_2^{2+} (aq), as a function of ξ.

used for the deprotonation reaction, an entropic energy correction of $-TS$, where the entropy (given as $S = k_B \ln 8$) must be added to the computed free-energy difference. At T = 300 K, this correction amounts to −1.24 kcal/mol, yielding the final estimate of the free-energy difference to be ΔF = 1.28 kcal/mol, and subsequently a pK_a value of 0.93 (eq 3). The simulated and experimental pK_a values of U^{4+}(aq) are reported in Table 5. The simulated pK_a value is greater than the

Table 5. p*K*a Values of U^{4+}(aq), UO_2^+ (aq), and UO_2^{2+} (aq)

	p*K*a			
	Simulation		Experiment	
	value	ref	value	ref
U^{4+}(aq)	0.93	this work	0.54	33
UO_2^+ (aq)	8.51	this work		
UO_2^{2+} (aq)	4.95	this work	5.24	33
	6.98	87	5.58	34
	9.61	39		
	−0.21	39		

experimental value by 0.4 pH units (experimental pK_a = 0.54 ± 0.06).[33] However, considering the fact that the experimental probes correspond to the infinite dilution limit—a condition which our model fails to satisfy, because of its finite size—we claim that the metadynamics simulation with the coordination number as a collective variable yields a pK_a value that is in reasonable agreement with the experiment.

UO_2^+(aq) and UO_2^{2+}(aq). The free-energy profiles in Figure 8 (red and blue curves) yield ΔF values of 12.64 kcal/mol for UO_2^+ and 7.75 kcal/mol for UO_2^{2+}. Accounting for the entropic correction of $-k_BT \ln 5$ = −0.96 kcal/mol results in the first-hydrolysis free energy of UO_2^+ being 11.68 kcal/mol and the pK_a value of UO_2^+ being 8.51. Similarly, the first-hydrolysis free energy and pK_a values of UO_2^{2+} are 6.79 kcal/mol and 4.95, respectively. The simulated and experimental pK_a values for UO_2^+ and UO_2^{2+} are summarized in Table 5. The simulated pK_a value for UO_2^{2+} deviates from one experimental value of 5.24 ± 0.25 (ref 33) by 0.3 pH units and another value of 5.58 ± 0.24 (ref 34) by 0.6 pH units. Again, if we consider the fact that the experimental value corresponds to the infinite dilution limit, then the simulated value agrees well with the experimental values. Also listed in Table 5 are the pK_a values of UO_2^{2+} from previous theoretical studies: 6.98 (ab initio MD simulation),[87] 9.61 (gas-phase simulation with BSJ dielectric

dx.doi.org/10.1021/ic202338z | Inorg. Chem. 2012, 51, 3016–3024

continuum model used to treat solvent effects),[39] and −0.21 (gas-phase simulation with a polarizable continuum model used to treat solvent effects).[88] Our pK_a value for UO_2^{2+} is the best theoretical value against the experiment and this gives us confidence in the predicted pK_a value for UO_2^{+}. Based on the deviations of the U^{4+} and UO_2^{2+} hydrolysis free energies from the experimental values (~0.5 and 1 kcal/mol, respectively), we conservatively estimate the error in the free energy of UO_2^{+} to be 1 kcal/mol; this translates to a pK_a error of 0.7 pH units.

4. SUMMARY AND CONCLUSIONS

Using density functional theory (DFT)-based constant-temperature (300 K) ab initio molecular dynamics (AIMD), we have elucidated the (i) hydration-shell geometries of UO_2^{+}(aq) and U^{4+}(aq) and (ii) water polarization properties and first hydrolysis of UO_2^{2+}, UO_2^{+}, and U^{4+}. These three ions are key players in uranium nuclear waste remediation, and this study has made contributions to our understanding of these ions in aqueous solution.

The first-hydration-shell geometry of UO_2^{+} is similar to that of UO_2^{2+} and it contains five water ligands in the equatorial plane, with average U═O_{ax} and U−O distances of 1.85 Å and 2.45 Å, respectively. The U═O_{ax} and U−O distances in UO_2^{+}(aq) are slightly elongated, in comparison to the corresponding distances in UO_2^{2+}(aq), because of reduced U−O electrostatic attraction. The second shell of UO_2^{+}(aq) contains an average of 15.4 water molecules at an average U−O distance of 4.55 Å. The equatorial and apical second shells respectively contain 8−9 and 6−7 water molecules.

UO_2^{+} polarizes the first-shell water molecules and causes an average dipole moment shift of 0.6 D, relative to the second-shell and bulk regions. UO_2^{2+} polarizes the water molecules even more (1.2 D, relative to bulk water). The first-shell water molecules of UO_2^{+} showed a fairly large average tilt angle of 35°, because of the presence of the neighboring second-shell and bulk waters and the strong first-shell UO_2^{+}−OH_2 electrostatic interaction. As a consequence of the large tilt angle, (i) the hydrogen bonding network between the first- and second-shell water molecules has some degree of tetrahedral character and (ii) the lone pair orbitals on each first-shell water molecule are asymmetrically positioned, relative to the position of the corresponding O atom. The asymmetric orientation of the first-shell water lone pair orbitals is also observed in UO_2^{2+}. The computed acidity constant of UO_2^{2+} to 4.95 is in good agreement with the experimental values of 5.24 ± 0.25 (ref 33) and 5.58 ± 0.24 (ref 34). We also predict, for the first time, that UO_2^{+} is a weak acid in solution with a pK_a value of 8.5. This result is particularly important: although thermodynamic data for UO_2^{+} is available, no data are available for hydrolyzed species. In effect, our work says that one can use UO_2^{+} in thermodynamic calculations, up to pH ~8.5 (excluding the presence of strongly interacting ligands).

The first shell of U^{4+} contains 8 or 9 water ligands. The weighted coordination number of 8.7 lies on the low end of the experimental range of 8−11.[46−49] The average first-shell U−O distance of 2.45 Å closely matches the reported experimental EXAFS values of 2.40 Å (ref 49) and 2.42 Å (ref 48) and the LAXS value of 2.45 Å.[46,47] The simulated EXAFS of U^{4+}(aq) is in good agreement with recent experimental data.[49] The average second-shell coordination number U^{4+} is 15.2, with a corresponding U−O distance of 4.65 Å. The average first-shell water molecule tilt angle is 24°, with the corresponding hydrogen bonding network between the second-shell acceptors and first-shell donors being predominantly trigonal. The strong polarization of the first-shell water molecules by U^{4+} results in an average dipole moment shift of 1.2 D, relative to the average bulk dipole moment. The simulated pK_a value of U^{4+} is 0.93, and this is in very good agreement with the experimental value of 0.54.

■ ASSOCIATED CONTENT

Ⓢ Supporting Information

Details of the metadynamics collective variable. The MD-EXAFS method. Hydrogen bonding analysis. EXAFS comparisons. First-shell deprotonation mechanisms. This material is available free of charge via the Internet at http://pubs.acs.org.

■ AUTHOR INFORMATION

Corresponding Author

*E-mails: Raymond.Atta-Fynn@pnnl.gov, Eric.Bylaska@pnnl.gov, Wibe.deJong@pnnl.gov.

Notes

The authors declare no competing financial interest.

■ ACKNOWLEDGMENTS

We are greatly indebted to Drs. Atsushi Ikeda-Ohno and Christoph Hennig for providing the experimental EXAFS data for U^{4+} and UO_2^{2+} in 1 M in $HClO_4$ solution. We also thank Drs. Henry Moll, Ingmar Grenthe, and Melissa Denecke for providing the experimental EXAFS data for U^{4+} in 1.5 M $HClO_4$ solution. This research was performed using the Molecular Science Computing Capability in the William R. Wiley Environmental Molecular Science Laboratory (EMSL), which is a national scientific user facility sponsored by the U.S. Department of Energy's Office of Biological and Environmental Research and located at the Pacific Northwest National Laboratory (PNNL), operated for the Department of Energy by Battelle. This research also used resources of the National Energy Research Scientific Computing Center (NERSC), which is supported by the Office of Science of the U.S. Department of Energy (under Contract No. DE-AC02-05CH11231). This research was supported by the BES Heavy Element Chemistry program and the Division of Chemical Sciences, Geo-Sciences, and Biosciences, Office of Basic Energy Sciences, U.S. Department of Energy.

■ REFERENCES

(1) Morris, D. E. *Inorg. Chem.* **2002**, *41*, 3542.
(2) Lovley, D. R.; Phillips, E. J. P.; Gorby, Y. A.; Landa, E. R. *Nature* **1991**, *350*, 413.
(3) Renshaw, J. C. *Environ. Sci. Technol.* **2005**, *39*, 5657.
(4) Lojou, E.; Bianco, P. J. *Electroanal. Chem.* **1999**, *471*, 96.
(5) Tucker, M. D.; Barton, L. L.; Thomson, B. M. *Appl. Microbiol. Biotechnol.* **1996**, *46*, 74.
(6) Tebo, B. M.; Obraztsova, A. Y. *FEMS Microbiol. Lett.* **1998**, *162*, 193.
(7) Truex, M. J.; Peyton, B. M.; Valentine, N. B.; Gorby, Y. A. *Biotechnol. Bioeng.* **1997**, *55*, 490.
(8) Spear, J. R.; Figueroa, L. A.; Honeyman, B. D. *Environ. Sci. Technol.* **1999**, *33*, 2667.
(9) Spear, J. R.; Figueroa, L. A.; Honeyman, B. D. *Appl. Environ. Microbiol.* **2000**, *66*, 3711.
(10) Tsezos, M.; Georgousis, Z.; Remoudaki, E. *Biotechnol. Bioengin.* **1997**, *55*, 16.
(11) Ilton, E. S.; Haiduc, A.; Cahill, C. L.; Felmy, A. R. *Inorg. Chem.* **2005**, *44*, 2986.

(12) Wersin, P.; Hochella, M. F.; Persson, P.; Redden, G.; Leckie, J. O.; Harris, D. W. *Geochim. Cosmochim. Acta* **1994**, *58*, 2829.
(13) Liger, E.; Charlet, L.; Van Cappellen, P. *Geochim. Cosmochim. Acta* **1999**, *63*, 2939.
(14) Charlet, L.; Silvester, E.; Liger, E. *Chem. Geol.* **1998**, *151*, 85.
(15) Baranger, P.; Disnar, J. R. *Bull. Soc. Geol. Fr.* **1991**, *162*, 271.
(16) McCleskey, T. M.; Foreman, T. M.; Hallman, E. E.; Burns, C. J.; Sauer, N. N. *Environ. Sci. Technol.* **2001**, *35*, 547.
(17) Wang, W. D.; Bakac, A.; Espenso, J. H. *Inorg. Chem.* **1995**, *34*, 6034.
(18) Sarakha, M.; Bolte, M.; Burrows, H. D. J. *Photochem. Photobiol. A* **1997**, *107*, 101.
(19) Eliet, V.; Bidoglio, G. *Environ. Sci. Technol.* **1998**, *32*, 3155.
(20) Cohen, D. J. *Inorg. Nucl. Chem.* **1970**, *32*, 3525.
(21) Ferri, D.; Grenthe, I.; Salvotore, F. *Inorg. Chem.* **1983**, *22*, 3162.
(22) Madic, C.; Hobart, D. E.; Begun, G. M. *Inorg. Chem.* **1983**, *22*, 1494.
(23) Mizuguchi, K.; Park, Y.-Y.; Tomiyasu, H.; Ikeda, Y. *J. Nucl. Sci. Technol.* **1993**, *30*, 542.
(24) Mizuoka, K.; Grenthe, I.; Ikeda, Y. *Inorg. Chem.* **2005**, *44*, 4472.
(25) Docrat, T. I.; Mosselmans, J. F. W.; Charnock, J. M.; Whiteley, M. W.; Collison, D.; Livens, F. R.; Jones, C.; Edmiston, M. J. *Inorg. Chem.* **1999**, *38*, 1879.
(26) Ikeda, A.; Hennig, C.; Tsushima, S.; Takao, K.; Ikeda, Y.; Scheinost, A. C.; Bernhard, G. *Inorg. Chem.* **2007**, *46*, 4212.
(27) Clark, D. L.; Hobart, D. E.; Neu, M. P. *Chem. Rev.* **1995**, *95*, 25.
(28) Horeglad, P.; Nocton, G.; Filinchuck, Y.; Pécaut, J.; Mazzanti, M. *Chem. Commun.* **2009**, 1843.
(29) Nocton, G.; Horeglad, P.; Vetere, V.; Pécaut, J.; Dubois, L.; Maldivi, P.; Edelstein, N.; Mazzanti, M. *J. Am. Chem. Soc.* **2010**, *132*, 495.
(30) Takao, K.; Tsushima, S.; Takao, S.; Scheinost, A. C.; Bernhard, G.; Ikeda, Y.; Hennig, C. *Inorg. Chem.* **2009**, *48*, 9602.
(31) Ilton, E. S.; Boily, J. F.; Buck, E. C.; Skomurski, F. N.; Rosso, K. M.; Cahill, C. L.; Bargar, J. R.; Felmy, A. R. *Environ. Sci. Technol.* **2010**, *44*, 170.
(32) Nichols, P.; Bylaska, E. J.; Schenter, G. K.; DeJong, W. A. *J. Chem. Phys.* **2008**, *128*, 124507.
(33) Guillaumont, R.; Fanghanel, T.; Fuger, J.; Grenthe, I.; Neck, V.; Palmer, D. A.; Rand, M. H. In *Update on the Chemical Thermodynamics of Uranium, Neptunium, Plutonium, Americium, and Technetium*; Mompean, F. J., Domenech-Orti, C., Ben Said, K., Illemassène, M., Eds.; Chemical Thermodynamics, Vol. 5; Elsevier: Amsterdam, 2003.
(34) Zanonato, P.; Bernardo, P. D.; Bismondo, A.; Liu, G.; Chen, X.; Rao, L. *J. Am. Chem. Soc.* **2004**, *126*, 5515.
(35) Allen, P. G.; B., J. J.; Shuh, D. K.; Edelstein, N. M.; Reich, T. *Inorg. Chem.* **1997**, *36*, 4676.
(36) Conradson, S. D. *Appl. Spectrosc.* **1998**, *52*, 252A.
(37) Ankudinov, A. L.; Conradson, S. D.; de Leon, J. M.; Rehr, J. J. *Phys. Rev. B* **1998**, *57*, 7518.
(38) Gagliardi, L.; Roos, B. O. *Chem. Phys. Lett.* **2000**, *331*, 229.
(39) Hay, P. J.; Martin, R. L.; Schreckenbach, G. *J. Phys. Chem. A* **2000**, *104*, 6259.
(40) Shamov, G. A.; Schreckenbach, G. *J. Phys. Chem. A* **2005**, *109*, 10961.
(41) Tsushima, S.; Wahlgren, U.; Grenthe, I. *J. Phys. Chem. A* **2006**, *110*, 9175.
(42) Austin, J. P.; Sundararajan, M.; Vincent, M. A.; Hillier, I. H. *J. Chem. Soc., Dalton Trans.* **2009**, 5902.
(43) Denning, R. *J. Phys. Chem. A* **2007**, *111*, 4125.
(44) Vallet, V.; Privalov, T.; Wahlgren, U.; Grenthe, I. *J. Am. Chem. Soc.* **2004**, *126*, 7766.
(45) Frick, R. J.; Hofer, T. S.; Pribil, A. B.; Randolf, B. R.; Rode, B. M. *Phys. Chem. Chem. Phys.* **2010**, *12*, 11736.
(46) Pocev, S.; Johansson, G. *Acta Chem. Scand.* **1973**, *27*, 2146.
(47) Johansson, G. In *Advances in Inorganic Chemistry, Vol. 39*; Sykes, A. G., Ed.; Academic Press: London, 1992.
(48) Moll, H.; Denecke, M. A.; Jalilehvand, M. A. F.; Sandström, M.; Grenthe, I. *Inorg. Chem.* **1999**, *38*, 1795.
(49) Ikeda-Ohno, A.; Hennig, C.; Tsushima, S.; Scheinost, A. C.; Bernhard, G.; Yaita, T. *Inorg. Chem.* **2009**, *48*, 7201.
(50) Tsushima, S.; Yang, T. *Chem. Phys. Lett.* **2005**, *401*, 68.
(51) Chaboy, J.; Díaz-Moreno, S. *J. Phys. Chem. A* **2011**, *115*, 2345.
(52) Frick, R. J.; Pribil, A. B.; Hofer, T. S.; Randolf, B. R.; Bhattacharjee, A.; Rode, B. M. *Inorg. Chem.* **2009**, *48*, 3993.
(53) Car, R.; Parrinello, M. *Phys. Rev. Lett.* **1985**, *55*, 2471.
(54) Kohn, W.; Sham, L. J. *Phys. Rev.* **1965**, *140*, A1133.
(55) Valiev, M.; Bylaska, E. J.; Govind, N.; Kowalski, K.; Straatsma, T. P.; van Dam, H. J. J.; Wang, D.; Nieplocha, J.; Apra, E.; Windus, T. L.; Jong, W. A. D. *Comput. Phys. Commun.* **2010**, *181*, 1477.
(56) Perdew, J. P.; Burke, K.; Ernzerhof, M. *Phys. Rev. Lett.* **1996**, *77*, 3865.
(57) Kleinman, L.; Bylander, D. M. *Phys. Rev. Lett.* **1982**, *48*, 1425.
(58) Hamann, D. R.; Schluter, M.; Chiang, C. *Phys. Rev. Lett.* **1979**, *43*, 1494.
(59) Hamann, D. R. *Phys. Rev. B* **1989**, *40*, 2980.
(60) Troullier, N.; Martins, J. L. *Phys. Rev. B* **1991**, *43*, 1993.
(61) Nose, S. *Mol. Phys.* **1984**, *52*, 255.
(62) Hoover, W. G. *Phys. Rev. A* **1985**, *31*, 1695.
(63) Cauët, E.; Bogatko, S.; Weare, J. H.; Fulton, J. L.; Schenter, G. K.; Bylaska, E. J. *J. Chem. Phys.* **2010**, *132*, 194502.
(64) Zwanzig, R. W. *J. Chem. Phys.* **1954**, *22*, 1420.
(65) Kirkwood, J. G. *J. Chem. Phys.* **1935**, *3*, 300.
(66) Straatsma, T. P.; McCammon, J. A. *J. Chem. Phys.* **1991**, *95*, 1175.
(67) Torrie, G. M.; Valleau, J. P. *J. Comput. Phys.* **1977**, *23*, 187.
(68) Micheletti, C.; Laio, A.; Parrinello, M. *Phys. Rev. Lett.* **2004**, *92*, 170601.
(69) Laio, A.; Parrinello, M. *Proc. Natl. Acad. Sci. U.S.A.* **2002**, *99*, 12562.
(70) Laio, A.; Gervasio, F. L. *Rep. Prog. Phys.* **2008**, *71*, 126601.
(71) Sprik, M. *Chem. Phys.* **2000**, *258*, 139.
(72) Farkas, I.; Grenthe, I.; Banyái, I. *J. Phys. Chem. A* **2000**, *104*, 1201.
(73) Wiebke, J.; Moritz, A.; Cao, X.; Dolg, M. *Phys. Chem. Chem. Phys.* **2007**, *9*, 459.
(74) Atta-Fynn, R.; Bylaska, E. J.; Schenter, G. K.; de Jong, W. A. *J. Phys. Chem. A* **2011**, *115*, 4665.
(75) Altmaier, M.; Cho, H. R.; Klenze, R.; Lindqvist-Reis, P.; Marquardt, C. M.; Neck, V.; Panak, P.; Seibert, A.; Walther, C.; Yun, J. I.; Fanghänel, T. In *Institute for Nuclear Waste Disposal: Annual Report*; Geckeis, H., Ed.; 2005; p 10.
(76) García-Hernández, M.; Lauterbach, C.; Krüger, S.; Matveev, A.; Rösch, N. *J. Comput. Chem.* **2002**, *23*, 834.
(77) Richens, D. T. *The Chemistry of Aqua Ions*; Wiley: Chichester, U.K., 1997.
(78) Rehr, J. J.; Albers, R. C. *Rev. Mod. Phys.* **2000**, *72*, 621.
(79) Rehr, J. J.; Kas, J. J.; Prange, M. P.; Sorini, A. P.; Takimoto, Y.; Vila, F. *C. R. Phys.* **2009**, *10*, 548.
(80) Palmer, B. J.; Pfund, D. M.; Fulton, J. L. *J. Phys. Chem.* **1996**, *100*, 13393.
(81) Wannier, G. H. *Phys. Rev.* **1937**, *52*, 0191.
(82) Foster, J. M.; Boys, S. F. *Rev. Mod. Phys.* **1960**, *32*, 300.
(83) Silvestrelli, P. L.; Marzari, N.; Vanderbilt, D.; Parrinello, M. *Solid State Commun.* **1998**, *107*, 7.
(84) Marzari, N.; Vanderbilt, D. *Phys. Rev. B* **1997**, *56*, 12847.
(85) Silvestrelli, P. L.; Parrinello, M. *Phys. Rev. Lett.* **1999**, *82*, 3308.
(86) Lightstone, F. C.; Schwegler, E.; Hood, R. Q.; Gygi, F.; Galli, G. *Chem. Phys. Lett.* **2001**, *343*, 549.
(87) Bühl, M.; Kabrede, H. *Inorg. Chem.* **2006**, *45*, 3834.
(88) Tsushima, S.; Yang, T.; Suzuki, A. *Chem. Phys. Lett.* **2001**, *334*, 365.